Available online at www.sciencedirect.com
SCIENCE DIRECT®
Journal of Solid State Chemistry 178 (2005) 3207–3217
JOURNAL OF SOLID STATE CHEMISTRY
www.elsevier.com/locate/jssc

High resolution and in situ neutron powder diffraction study of the crystal structure and the stability of $Ba_4CaCu_3O_{8+\delta}$

H. Nguyen Xuan[a], Ph. Galez[a,*], A. Pisch[b], Ch. Bertrand[a], S. Beauquis[a], J.L. Soubeyroux[c], F. Bourée-Vigneron[d]

[a]*LAIMAN-ESIA, Université de Savoie, BP 806, F-74016 Annecy Cedex, France*
[b]*LTPCM, UMR 5614, CNRS-INPG-UJF, 1130 Rue de la Piscine, F-38402 Saint Martin d'Hères, France*
[c]*Laboratoire de Cristallographie, CNRS, BP 166, F-38042 Grenoble Cedex 9, France*
[d]*LLB, CEA-CNRS, CEA-Saclay, F-91191 Gif-sur-Yvette, France*

Received 14 April 2005; received in revised form 30 June 2005; accepted 15 July 2005
Available online 6 September 2005

Abstract

The crystal structure and stability of $Ba_4CaCu_3O_{8+\delta}$ have been investigated by neutron powder diffraction, differential thermal analysis and thermogravimetry. It is found that the phase is not stable below 1065 K in $p(O_2) = 1$ bar and decomposes according to the eutectoid reaction $Ba_4CaCu_3O_{8+\delta} + x\ O_2 \Rightarrow Ba_2CuO_{3.4} + CaO + 2BaCuO_2$. However, the equilibrium with the outer gas is not reached for sintered ceramics so that $Ba_4CaCu_3O_{8+\delta}$ can be obtained in a metastable state after normal cooling conditions. In this case, the crystal structure is cubic (*Im*-3*m*, $a = 8.1452(1)$ Å, $\delta = 0.68$, $Z = 2$, $R_{wp} = 2.5\%$, $R_{Bragg} = 5.4\%$) as reported in the literature. In reduced oxygen partial pressure ($p(O_2) < 10^{-6}$ bar), $Ba_4CaCu_3O_{8+\delta}$ is stable down to room temperature and has a tetragonal structure with a significant lower oxygen content (*P*4/*mmm*, $a = 8.1976(3)$ Å, $c = 8.0709(3)$ Å, $\delta = -0.81$, $Z = 2$, $R_{wp} = 2.8\%$, $R_{Bragg} = 5.1\%$). The difference between the two crystal structures is discussed in terms of oxygen content, copper formal valence and cation coordination. The influence of the oxygen pressure on the stability of $Ba_4CaCu_3O_{8+\delta}$ is also discussed.

Keywords: Powders-solid state reaction; Neutron powder diffraction; Thermal stability; Thermodynamic properties; $Ba_4CaCu_3O_{8+\delta}$

1. Introduction

The fabrication of Tl- and Hg-based high-T_c superconducting cuprates with optimised and reproducible properties requires a thorough knowledge of the complex Tl–Ba–Ca–Cu–O and Hg–Ba–Ca–Cu–O systems and of their numerous subsystems. Among them, the BaO–CaO–CuO system is of particular interest since, in most cases, Tl- and Hg-based superconducting films are prepared by thallination or mercuration of a Ba–Ca–Cu–O precursor of appropriate composition. It was investigated in the early 1990s by several groups [1–4] which resulted in the discovery of two ternary compounds: $Ba_4CaCu_3O_{8+\delta}$ and $Ba_6CaCu_3O_{10+\delta}$ with a cubic ($a = 8.12-8.15$ Å) and a tetragonal structure ($a = 4.06$ Å and $c = 21.61$ Å), respectively.

The 413 phase was first identified by Greaves and Slater [1]. These authors showed that its crystal structure is closely related to the structure of $Ba_4YCu_3O_{8.5+\delta}$ [5] with, however, some differences in oxygen order. They proposed a model of atom arrangement in space group *Im*-3*m* which was later confirmed by Kubat-Martin et al [4]. The structure is derived from the perovskite-type structure. The large Ba atoms occupy the 12-fold coordinated sites (12co) whereas the calcium and copper atoms occupy the six-fold coordinated sites (6o) in an ordered manner which gives rise to the eight-fold

*Corresponding author. Laboratoire d'Instrumentation et des Matériaux d'Annecy, ESIA-Université de Savoie, BP 806, F-74016 Annecy cedex, France. Fax: +33 4 50 09 66 49.
E-mail address: philippe.galez@univ-savoie.fr (P. Galez).

0022-4596/$ - see front matter © 2005 Elsevier Inc. All rights reserved.
doi:10.1016/j.jssc.2005.07.010

superstructure ($2a$, $2a$, $2a$) with respect to the standard perovskite cell (Fig. 1). The oxygen positions around the Ca atoms are fully or almost fully occupied whereas the oxygen positions located between Cu atoms are only half occupied which results in an overall O content of 8.6–8.8 per formula unit. Note that Abbattista et al. [3] used the same space group (Pm-3) and the same oxygen order as in the structure of $Ba_4YCu_3O_{8.5+\delta}$ to account for their X-ray diffraction data.

The 613 phase was first identified by the latter authors [3] and found isostructural to $Ba_6YCu_3O_{10.5+\delta}$ ($I4/mmm$) [6], i.e. isostructural to the second member of the Ruddlesden-Popper series. The overall oxygen content, ≈ 10.5 per formula unit to be compared with 14 if all O sites were fully occupied, is due to a partial occupancy of the oxygen positions located in the equatorial plane of the (Cu,Ca)O_6 octahedra. A third ternary compound with composition Ba_2CaCuO_4 was reported by Lin and Wu [7] but its diffraction pattern was later assigned to $Ba_4CaCu_2O_{7+\delta}(CO_3)$ [8].

In a recent work [9], we showed that both $Ba_4CaCu_3O_{8+\delta}$ and $Ba_6CaCu_3O_{10+\delta}$ phases are metastable at room temperature in $p(O_2) = 1$ bar. From differential thermal analysis (DTA) and thermogravimetry analysis (TGA), we inferred that they undergo a decomposition into BaO_2, CaO and $Ba_2Cu_3O_6$ at about 985 K according to the following eutectoid reactions:

$$Ba_4CaCu_3O_{8+\delta} \rightarrow 2BaO_2 + CaO + Ba_2Cu_3O_6$$

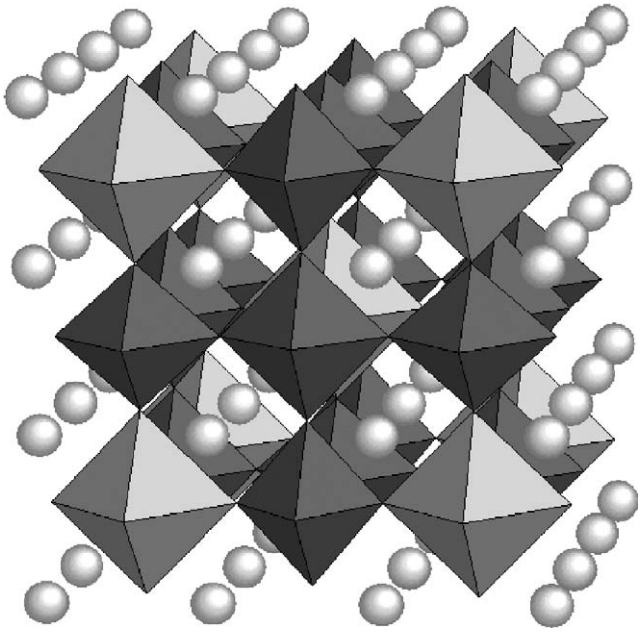

Fig. 1. Schematic representation of the structure of cubic $Ba_4CaCu_3O_{8+\delta}$. CuO_6 octahedra: dark grey; CaO_6 octahedra and Ba atoms: light grey. The oxygen positions located between copper atoms are only half occupied which gives a total of four O neighbours per copper atom in an octahedral coordination.

and

$$Ba_6CaCu_3O_{10+\delta} \rightarrow 4BaO_2 + CaO + Ba_2Cu_3O_6.$$

The occurrence of these decompositions strongly depends on the sintering state of the ceramics. The equilibrium with the outer oxygen gas is not reached when the ceramics are very dense so that the eutectoid reactions do not occur. Therefore, both $Ba_4CaCu_3O_{8+\delta}$ and $Ba_6CaCu_3O_{10+\delta}$ phases can be obtained after a high temperature treatment with normal cooling conditions. The same phenomenon was observed for $Ba_2CuO_{3+\delta}$ [10].

We also proposed from X-ray diffraction data [11] a tetragonal structure ($I4/mmm$) for $Ba_4CaCu_3O_{8+\delta}$ when it is prepared in an inert atmosphere.

This report focuses on the stability and the crystal structure of $Ba_4CaCu_3O_{8+\delta}$. High resolution neutron powder diffraction data were used to refine the crystal structure of both cubic and tetragonal $Ba_4CaCu_3O_{8+\delta}$ with an emphasis on the oxygen order. In addition, the sequence of phase transformations in an initially tetragonal $Ba_4CaCu_3O_{8+\delta}$ ceramic sample was followed by in situ neutron powder diffraction from room temperature to 1120 K in $p(O_2) = 1$ bar in order to confirm the above mentioned interpretation of DTA/TGA results.

2. Experimental

2.1. Sample preparation

Bulk samples with composition Ba:Ca:Cu = 4:1:3 were prepared by solid state reaction in open system at 1170–1220 K from BaO_2, CuO and pre-fired CaO. High temperature treatments as long as 100 h with intermediate grindings were necessary to obtain almost pure 413 in both flowing oxygen and nitrogen.

The tetragonal distortion observed when the samples are prepared in low $p(O_2)$ is closely related to the oxygen content and strongly depends on the sintering conditions. It is all the more pronounced that the oxygen partial pressure is reduced. It may happen that, with standard quality nitrogen ($p(O_2) < 2 \times 10^{-6}$ atm.), the distortion be extremely small and hardly detectable. In order to maximise it, the oxygen partial pressure was further lowered by placing a titanium sponge in the nitrogen gas path.

In the following, the sample prepared in flowing oxygen will be referred to as 413-O_2 and the sample prepared in flowing nitrogen with a Ti sponge will be labelled 413-N_2. For a good counting statistics during the neutron diffraction experiments, about 9 g were prepared in each case which represent 6 pellets, 8 mm in diameter and 10 mm in height. To avoid degradation by air moisture [11], these pellets were sealed in a quartz tube under vacuum immediately after sintering.

2.2. Neutron diffraction

Room temperature neutron data was collected from 413-O_2 and 413-N_2 in their protective quartz tube either on the high resolution diffractometer 3T2 at the Laboratoire Léon Brillouin (LLB, Saclay; $\lambda = 1.2258$ Å, Ge (335) monochromator, $0° < 2\theta \leqslant 125°$, $0.05°$ 2θ step) or on the corresponding diffractometer D2B at the Institut Laue Langevin (ILL, Grenoble; $\lambda = 1.5942$ Å, Ge (335) monochromator, $0° < 2\theta \leqslant 161°, 0.05°$ 2θ step). In both cases, the neutron wavelength was refined with the cell parameters deduced from X-ray data (Cu$K\alpha$) collected from the same samples. The crystal structures were refined using the program Fullprof 2000 [12]. The following impurity phases were detected: $CaCO_3$, $BaCuO_2$ and CaO in 413-O_2 and $BaCu_2O_2$, $BaCuO_2$ and CaO in 413-N_2. They were all included in the refinements. Details on the procedure are given in Section 3.1.

Variable temperature neutron data in flowing oxygen was further collected from sample 413-N_2 on the high flux powder diffractometer D1B at the ILL ($\lambda = 2.524$ Å, Graphite (002) monochromator, $44° < 2\theta \leqslant 124°, 0.2°$ 2θ step). The sample was coarsely ground prior to heating to ensure equilibrium with the oxygen gas. The experimental set-up used to allow a good circulation of the oxygen gas through the sample yielded a significant underestimation of the sample temperature with respect to earlier DTA/TGA results [9]. A comparison between the two techniques showed that this underestimation reached 80 K at 1000 K. This could be due either to the high gas flow or to an oxygen pressure different from 1 bar during the neutron experiment (see Section 4.2). The collection time for a single pattern was set at 5 min. The temperature was rapidly (10 K/min) raised to 450 K and then the heating rate was reduced to 2 K/min until the maximum temperature, 1120 K, was reached. The sample was held at this temperature for a few minutes. At this point, the sample container broke so that no diffraction pattern could be recorded on cooling the sample. After a careful examination of the collected data, all reflections of all patterns could attributed to one of the following phases: tetragonal $Ba_4CaCu_3O_{8+\delta}$, cubic $Ba_4CaCu_3O_{8+\delta}$, CaO, BaO_2, low temperature and high temperature forms of $Ba_2Cu_3O_6$ (LT-$Ba_2Cu_3O_6$ and HT-$Ba_2Cu_3O_{6-\delta}$, respectively) [13,14], $Ba_2CuO_{3+\delta}$ (oxygen-rich orthorhombic form) [15] and $BaCuO_2$. Because the structures of both LT- and HT-$Ba_2Cu_3O_{6-\delta}$ are not known in details so far, we could not perform full profile Rietveld analysis on the set of diffraction patterns. However, qualitative results, obtained with the aid of the program LAMP [16] and by considering the integrated intensity of some characteristic peaks, are given below. This data analysis proved to be sufficient to have a precise picture of the phase transformation sequence.

3. Results

3.1. Structure refinement of cubic and tetragonal $Ba_4CaCu_3O_{8+\delta}$

Although the 413 phase is not stable at room temperature in $p(O_2) = 1$ bar, almost pure samples can be prepared without quenching from high temperature. This behaviour is attributed to the densification of the ceramics during sintering which does not allow a rapid equilibrium with the outer oxygen gas when the sample is cooled i.e. the oxygen partial pressure experienced by the individual grains is by far lower than the external oxygen pressure. The diffraction pattern of 413-O_2 was recorded on the 3T2 spectrometer of the LLB. The sample was found to contain $BaCuO_2$, $CaCO_3$ and CaO as impurity phases. The set of diffraction peaks due to $Ba_4CaCu_3O_{8+\delta}$ was satisfactorily indexed using a body centred cubic cell with $a \approx 8.15$ Å. No reflection violating the systematic extinction condition $h + k + l = 2n$ could be detected. The crystal structure was refined in space group $Im\text{-}3m$ using the published parameters [1,4] as input parameters. The background was set manually to account for the blurred maxima due to quartz around $2\theta = 13°$, $34°$ and $62°$ and the pseudo-Voigt function was used for peak fitting. Only the scale factor and the cell parameters were allowed to vary for the impurity phases: their asymmetry, mixing and profile shape coefficients were constrained to those of the main $Ba_4CaCu_3O_{8+\delta}$ phase. The refinement was based on diffraction data in the range $15° \leqslant 2\theta \leqslant 125°$ containing 119 reflections from cubic $Ba_4CaCu_3O_{8+\delta}$, 143 from $CaCO_3$, 1065 from $BaCuO_2$ and 21 from CaO. Final profile and Bragg agreement factors are given in Table 1 together with the weight fractions and the cell parameters for each phase. The final positional, occupational and isotropic displacement parameters for cubic $Ba_4CaCu_3O_{8+\delta}$ are given in Table 2. They are extremely close to those given by Greaves and Slater [1] and Kubat-Martin et al. [4]. Selected interatomic distances with average coordination numbers (ACNs) are reported in Table 3 and the observed, calculated and difference patterns are shown in Fig. 2a.

Because of the presence of $CaCO_3$ in the sample, attempts were made with $Ba_4CaCu_3O_{8+\delta}$ replaced by one of the related oxycarbonate phases reported in the literature [8,17–19] but remained unsuccessful. They systematically led to refinement instabilities and/or to unphysical occupational and displacement parameters and to large R factors. Refinements were also carried out in space groups $Pm\text{-}3$ and $P23$ which have been used to describe the structures of $Ba_4RECu_3O_z$ [5,20,21]. They resulted either in instabilities or in parameters fully compatible with higher symmetry space group $Im\text{-}3m$.

The crystal structure of tetragonal $Ba_4CaCu_3O_{8+\delta}$ was refined in the same manner using data collected on

Table 1
Weight fraction and cell parameters of the individual phases in 413-O_2 and 413-N_2

	413-O_2	413-N_2
R_p (%)	2.06	2.12
R_{wp} (%)	2.48	2.83
χ^2	2.31	2.56
Main phase	Cubic $Ba_4Ca_{0.92}Cu_3O_{8.68}$, $Z = 2$	Tetragonal $Ba_4CaCu_{2.93}O_{7.19}$, $Z = 2$
Space group	*Im*-3*m*	*P*4/*mmm*
Weight fraction (%)	89(2)	97(2)
a (Å)	8.1452(1)	8.1976(3)
c (Å)	—	8.0709(3)
V (Å^3)	540.38(3)	542.37(6)
R_{Bragg} (%)	5.38	5.07
Number of reflections	119	374
Secondary phase	$CaCO_3$, $Z = 6$, *R*-3*c*	$BaCu_2O_2$, $Z = 4$, $I4_1/amd$
Weight fraction (%)	6(1)	1.6(3)
a (Å)	4.9898(7)	5.738(3)
c (Å)	17.074(4)	10.04(1)
V (Å^3)	368.1(3)	330.7(7)
Number of reflections	143	100
$BaCuO_2$, $Z = 90$, *Im*-3*m*		
Weight fraction (%)	5(1)	1.0(3)
A (Å)	18.300(4)	18.28(2)
c (Å)	—	—
V (Å^3)	6128(6)	6104(15)
Number of reflections	1065	650
CaO, $Z = 4$, *Fm*-3*m*		
Weight fraction	0.11(6)	0.4(1)
a (Å)	4.808(1)	4.814(1)
V (Å^3)	111.1(1)	111.5(1)
Number of reflections	21	13

Table 2
Atom coordinates, isotropic displacement parameters (Å^2) and site occupancies in the structure of cubic and tetragonal $Ba_4CaCu_3O_{8+\delta}$

Atom	WP	*x*	*y*	*z*	*B*(Å^2)	Occ.
Cubic $Ba_4Ca_{0.92}Cu_3O_{8.68}$, $Z = 2$, I*m*-3*m*, Sample 413-O_2, LLB, $\lambda = 1.2258$ Å						
Ba	8(*c*)	1/4	1/4	1/4	1.74(5)	—
Ca	2(*a*)	0	0	0	1.3(3)	0.92(4)
Cu	6(*b*)	0	1/2	1/2	1.66(7)	—
O1	12(*e*)	0.2795(8)	0	0	2.48(8)	0.95(1)
O2	12(*d*)	1/4	0	1/2	3.6(2)	0.50(1)
Tetragonal $Ba_4CaCu_{2.93}O_{7.19}$, $Z = 2$, *P*4/*mmm*, Sample 413-N_2, ILL, $\lambda = 1.5942$ Å						
Ba	8(*r*)	0.2545(6)	0.2545(6)	0.2391(6)	1.57(5)	—
Ca1	1(*a*)	0	0	0	1.2(1)	—
Ca2	1(*d*)	1/2	1/2	1/2	1.2(1)	—
Cu1	1(*b*)	0	0	1/2	1.5(3)	—
Cu2	1(*c*)	1/2	1/2	0	0.8(3)	0.94(3)
Cu3	2(*f*)	0	1/2	0	1.5(2)	—
Cu4	2(*e*)	0	1/2	1/2	1.2(2)	0.96(2)
O1	4(*l*)	0.277(1)	0	0	2.2(2)	0.96(2)
O2	4(*o*)	0.781(1)	1/2	1/2	1.9(2)	—
O3	2(*g*)	0	0	0.278(2)	3.8(4)	0.95(3)
O4	2(*h*)	1/2	1/2	0.773(2)	1.9(2)	0.92(3)
O5	4(*n*)	0.235(2)	1/2	0	2.9(2)	0.65(2)
O6	16(*u*)[a]	0.049[b]	0.535[b]	0.284[b]	2.7[b]	0.014(4)

[a]Displaced from ideal position 4(*i*) 0 1/2 *z*.
[b]Not refined during the last cycles.

Table 3
Selected interatomic distances in the structure of cubic and tetragonal Ca-413 with the average coordination numbers (ACN)

Cubic $Ba_4Ca_{0.92}Cu_3O_{8.68}$, *Im*-3*m*	Tetragonal $Ba_4CaCu_{2.93}O_{7.19}$, *P*4/*mmm*	
Ba–O1 2.890(2) × 6 × 0.95	Ba–O1 2.848(6) × 2 × 0.96	Cu1–O3 1.79(1) × 2 × 0.95
Ba–O2 2.8797(1) × 6 × 0.50	Ba–O2 2.927(5) × 2	**ACN(Cu1) = 1.90**
⟨Ba–O⟩ = 2.89	Ba–O3 2.967(5) × 1 × 0.95	
ACN(Ba) = 8.70	Ba–O4 2.848(5) × 1 × 0.92	Cu2–O4 1.834(8) × 2 × 0.92
	Ba–O5 2.793(8) × 2 × 0.65	Cu2–O5 2.17(1) × 4 × 0.65
Ca-O1 2.277(3) × 6 × 0.95	Ba–O6 2.88(1) × 2 × 0.014	⟨Cu2–O⟩ = 2.03
ACN(Ca) = 5.70	Ba–O6 2.44(1) × 2 × 0.014	**ACN(Cu2) = 4.44**
	Ba–O6 3.05(1) × 2 × 0.014	
Cu–O1 1.796(4) × 2 × 0.95	⟨Ba–O⟩ = 2.88	Cu3–O1 1.8295(1) × 2 × 0.96
Cu–O2 2.0363(1) × 4 × 0.50	**ACN(Ba) = 7.17**	Cu3–O5 1.93(1) × 2 × 0.65
⟨Cu–O⟩ = 1.92		Cu3–O6 2.3(1) × 8 × 0.014
ACN(Cu) = 3.90	Ca1–O1 2.269(7) × 4 × 0.96	⟨Cu3–O⟩ = 1.88
	Ca1–O3 2.247(12) × 2 × 0.95	**ACN(Cu3) = 3.33**
	⟨Ca1–O⟩ = 2.26	
	ACN(Ca1) = 5.74	Cu4–O2 1.795(6) × 2
		Cu4–O6 1.8(1) × 8 × 0.014
	Ca2–O2 2.304(7) × 4	⟨Cu4–O⟩ = 1.80
	Ca2–O4 2.200(8) × 2 × 0.92	**ACN(Cu4) = 2.11**
	⟨Ca2–O⟩ = 2.27	
	ACN(Ca2) = 5.84	

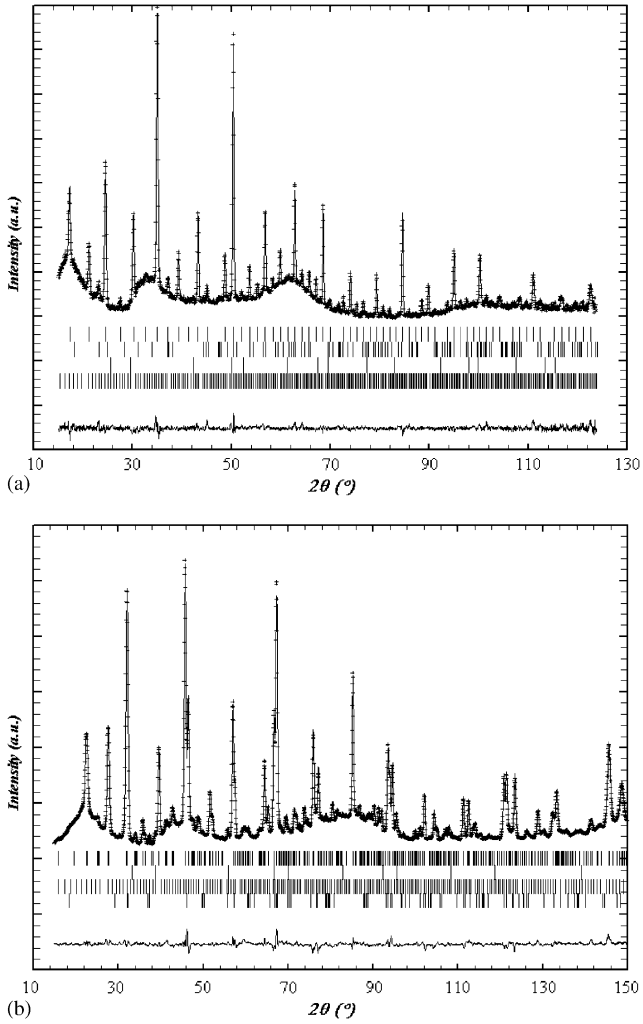

Fig. 2. Observed (+ symbols), calculated (full curve) and difference (bottom) diffraction patterns for (a) 413-O_2 and (b) 413-N_2.

D2B from 413-N_2. The sample was found to contain small amounts of $BaCu_2O_2$, $BaCuO_2$ and CaO as impurity phases. A close examination of the diffraction pattern also revealed the unambiguous presence of reflections violating the systematic extinction condition for a body centred Bravais lattice. The structure of tetragonal $Ba_4CaCu_3O_{8+\delta}$ cannot be described in space group *I*4/*mmm* as we mistakenly reported in Ref. [11] from X-ray data. A new structure model was derived in space group *P*4/*mmm*. The refinement in this particular space group yielded very good agreement factors and no improvement was encountered when space groups with lower symmetry and compatible with reflection conditions such as *P*4*mm*, *P*4/*m* or *P*4 were tested. It was based on diffraction data in the range $15^\circ \leqslant 2\theta \leqslant 150^\circ$ containing 374 reflections from tetragonal $Ba_4CaCu_3O_{8+\delta}$, 100 from $BaCu_2O_2$, 650 from $BaCuO_2$ and 13 from CaO. The results are given in Tables 1 and 2. Selected interatomic distances with ACNs are reported in Table 3 and the observed, calculated and difference patterns are shown in Fig. 2b.

3.2. *In situ* neutron diffraction experiment

The whole experiment can be displayed in a simple 2D graph (Fig. 3) [16] where each intensity value corresponds to a particular shade. This diagram may be seen as an assembly of Guinier films put on top of each other with the Bragg angle (2θ) as the abscissa and time or temperature as the ordinate. Using this graph, the reflections which appear and disappear at the same time are grouped into families so that the different phases present in the sample can be detected. Besides the starting tetragonal $Ba_4CaCu_3O_{8+\delta}$ phase, seven

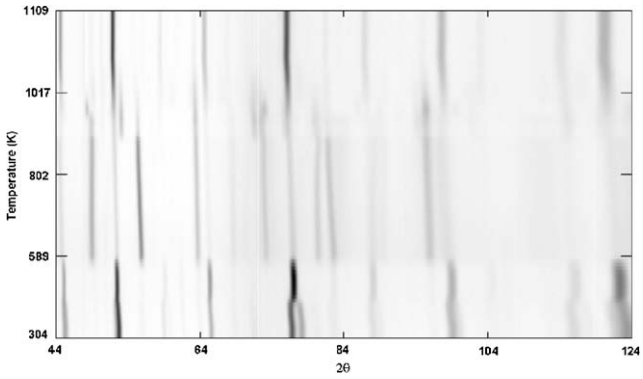

Fig. 3. 2D representation of the in situ diffraction experiment. The temperature indicated is as-measured (see text).

compounds were observed during the experiment: cubic $Ba_4CaCu_3O_{8+\delta}$, CaO, BaO_2, LT-$Ba_2Cu_3O_6$, HT-$Ba_2Cu_3O_6$, $Ba_2CuO_{3+\delta}$ and $BaCuO_2$. The information is summarised in Figs. 4 and 5 where the normalised integrated intensities of characteristic peaks are plotted as a function of the as-measured temperature.

The first noticeable event is the transformation from tetragonal to cubic $Ba_4CaCu_3O_{8+\delta}$ at $T \approx 430$ K. This is evidenced by significant and abrupt changes in the integrated intensity of both 220/202 and 222 reflections (Fig. 4) and by the clear merging of the 400 and 004 peaks at $2\theta \approx 76^\circ$ (Fig. 6). Then comes the expected decomposition of cubic $Ba_4CaCu_3O_{8+\delta}$ into CaO, BaO_2 and LT-$Ba_2Cu_3O_6$ at $T \approx 540$ K

$$Ba_4CaCu_3O_{8+\delta} \Rightarrow 2BaO_2 + CaO + \text{LT-}Ba_2Cu_3O_6.$$

Note that the decomposition is not complete which means that some ceramic pieces are dense enough to prevent equilibrium with the outer oxygen gas. These first two transformations, tetragonal $Ba_4CaCu_3O_{8+\delta} \Rightarrow$ cubic $Ba_4CaCu_3O_{8+\delta}$ and cubic $Ba_4CaCu_3O_{8+\delta} \Rightarrow 2\ BaO_2 + CaO + \text{LT-}Ba_2Cu_3O_6$, correspond to equilibrium recoveries with exothermic events in the DTA curve between 570 and 620 K and large associated oxygen uptakes (Fig. 7). They are not associated with intrinsic reaction temperatures and fully confirm that $Ba_4CaCu_3O_{8+\delta}$ is not a stable phase at low temperature in $p(O_2) = 1$ bar. The resulting equilibrium with BaO_2, CaO and LT-$Ba_2Cu_3O_6$ as solid phases, remains unchanged until $T \approx 860$ K (Fig. 5) when the following sequence of transformations lead *in fine* to the formation of cubic $Ba_4CaCu_3O_{8+\delta}$:

(a) First, BaO_2 and half of LT-$Ba_2Cu_3O_6$ react to form $Ba_2CuO_{3+\delta}$ according to the reaction:

$$2BaO_2 + \tfrac{1}{2}\text{LT} - Ba_2Cu_3O_6 \Rightarrow \tfrac{3}{2}Ba_2CuO_{3+\delta}.$$

This leads to the presence of CaO (1), LT-$Ba_2Cu_3O_6$ ($\frac{1}{2}$) and $Ba_2CuO_{3+\delta}$ ($\frac{3}{2}$). Between parentheses are the numbers of moles of each compound for 1 mole of $Ba_4CaCu_3O_{8+\delta}$ at the beginning of the experiment. This reaction is evidenced by the simultaneous ($T = 880$–920 K; Fig. 5) changes in the characteristic normalised intensities of BaO_2 (decrease from 1 to 0), LT-$Ba_2Cu_3O_6$ (decrease from 1 to $\frac{1}{2}$) and $Ba_2CuO_{3+\delta}$ (increase from 0 to 1). It corresponds to the first endothermic peak and the associated weight loss in the DTA/TGA curves (Fig. 7).

(b) Then, LT-$Ba_2Cu_3O_6$ is transformed into HT-$Ba_2Cu_3O_{6-\delta}$ [13,14] at $T \approx 950$ K (Fig. 5) resulting in the presence of CaO (1), HT-$Ba_2Cu_3O_{6-\delta}$ ($\frac{1}{2}$) and $Ba_2CuO_{3+\delta}$ ($\frac{3}{2}$).

(c) This is followed by a reaction between HT-$Ba_2Cu_3O_{6-\delta}$ and part of $Ba_2CuO_{3+\delta}$:

$$\tfrac{1}{2}Ba_2CuO_{3+\delta} + \tfrac{1}{2}\text{HT-}Ba_2Cu_3O_{6-\delta} \Rightarrow 2BaCuO_2$$

which gives a new equilibrium with $Ba_2CuO_{3+\delta}$ (1), CaO (1) and $BaCuO_2$ (2) as solid phases.

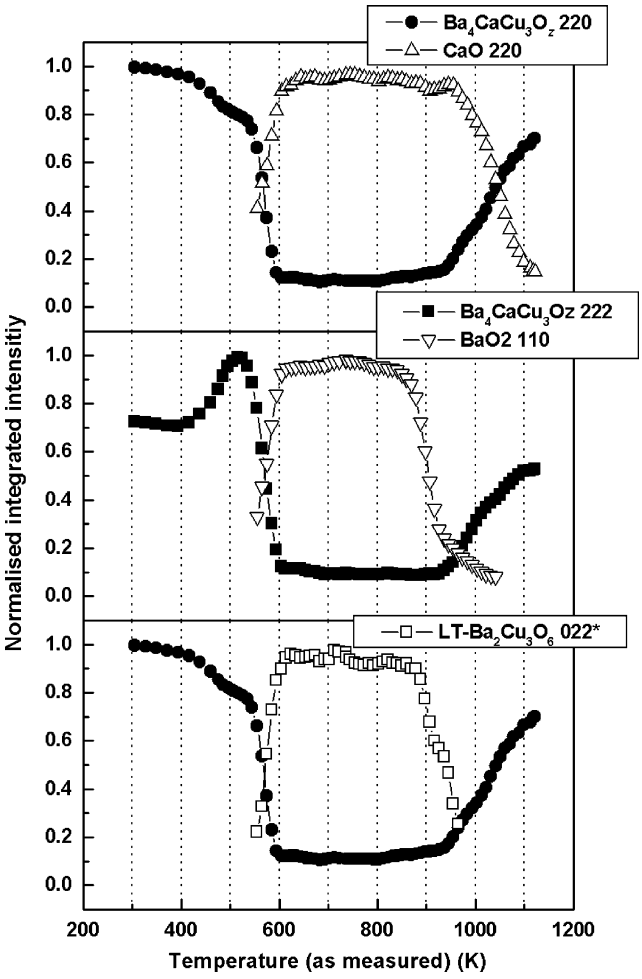

Fig. 4. Normalised integrated intensities as a function of temperature (as-measured) for several characteristic reflections showing the low temperature decomposition and the high temperature formation of $Ba_4CaCu_3O_{8+\delta}$.

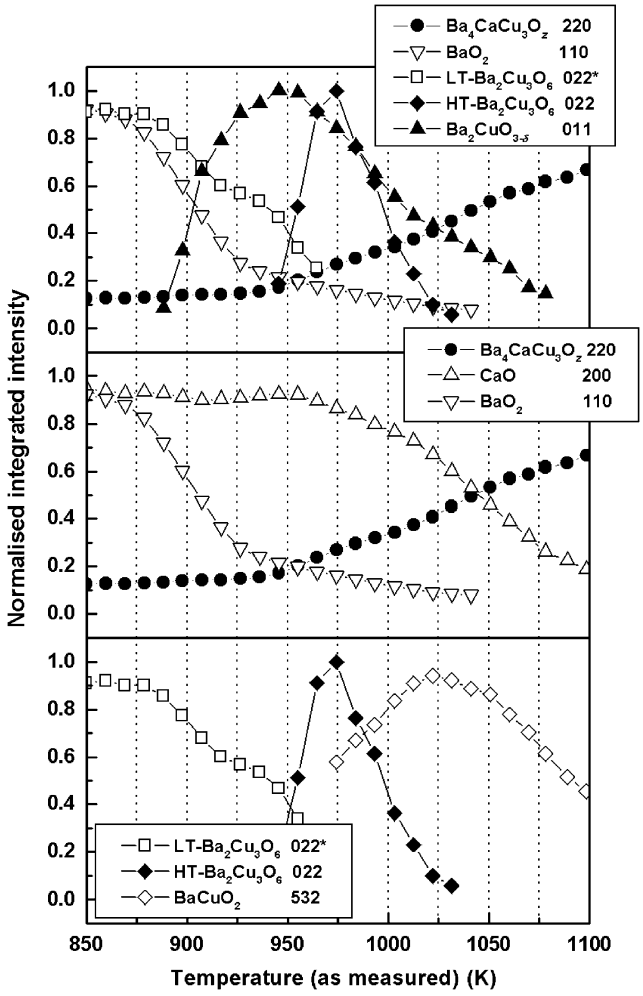

Fig. 5. Normalised integrated intensities as a function of temperature (as-measured) for several characteristic reflections with a focus on the formation of the $Ba_4CaCu_3O_{8+\delta}$ phase above 850 K.

(d) Finally, the three remaining oxides react to form cubic $Ba_4CaCu_3O_{8+\delta}$:

$$2BaCuO_2 + CaO + Ba_2CuO_{3+\delta} \Rightarrow \text{cubic } Ba_4CaCu_3O_{8+\delta}.$$

The two latter transformations almost occur simultaneously above $T = 980$ K i.e. cubic $Ba_4CaCu_3O_{8+\delta}$ starts to form while HT-$Ba_2Cu_3O_{6-\delta}$ decomposes and reacts with $Ba_2CuO_{3+\delta}$ to give $BaCuO_2$.

As already mentioned, the sample temperature was significantly underestimated during the experiment so that the values given above must not be considered. However, the reaction temperatures are precisely given by DTA/TGA results (Fig. 7). One finds 985 K (a), 1040–1050 K (b) and 1055–1065 K (c and d) at $p(O_2) = 1$ bar. The results are summarised in Table 4. The Fig. 8 shows a composition pyramid with the locations of the phases involved in the decomposition of $Ba_4CaCu_3O_{8+\delta}$ and the plane delimited by the solid phases in equilibrium with the oxygen gas below 985 K in $p(O_2) = 1$ bar.

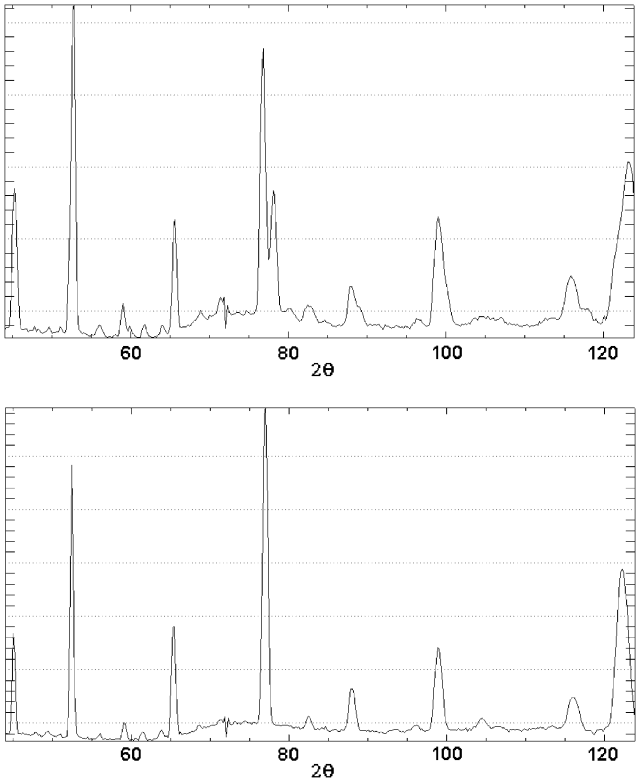

Fig. 6. Diffraction patterns recorded at 300 K (top) and 525 K (bottom), i.e. below and above the transformation from tetragonal to cubic $Ba_4CaCu_3O_{8+\delta}$.

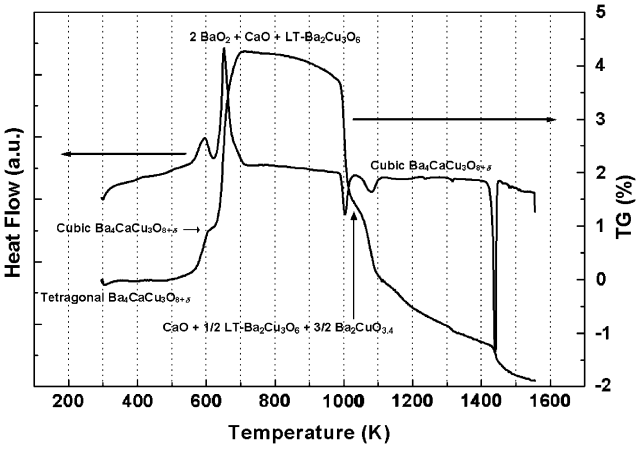

Fig. 7. DTA/TGA ($p(O_2) = 1$ bar) curves of a 60 mg powdered sample prepared in the same manner as 413-N_2. The two exothermic events at low temperature denote equilibrium recoveries. They are associated with substantial weight gains and correspond to the transformation from tetragonal to cubic $Ba_4CaCu_3O_{8+\delta}$ and to the decomposition cubic $Ba_4CaCu_3O_{8+\delta} \Rightarrow BaO_2 + CaO + LT\text{-}Ba_2Cu_3O_6$. The higher temperature endotherms correspond to the sequence of transformations which lead to the formation of cubic $Ba_4CaCu_3O_{8+\delta}$.

Table 4
Phases and reactions found on heating the sample during the in situ neutron powder diffraction experiment

Temperature (K)	Observed phases			Reactions
300–570	Tetragonal $Ba_4CaCu_3O_z$ (metastable)			
570				Tetragonal $Ba_4CaCu_3O_z + x\ O_2 \Rightarrow$ cubic $Ba_4CaCu_3O_z$
570–620	Cubic $Ba_4CaCu_3O_z$ (metastable)			
620				cubic $Ba_4CaCu_3O_z + x\ O_2 \Rightarrow 2BaO_2 + LT\text{-}Ba_2Cu_3O_6 + CaO$
600–985	BaO_2, (2)	LT-$Ba_2Cu_3O_6$, (1)	CaO (1)	
	Solid phases at equilibrium with 1 bar O_2 (300–985 K)			
985				$2BaO_2 + \frac{1}{2}LT - Ba_2Cu_3O6 \Rightarrow \frac{3}{2}Ba_2CuO_{3.4} + xO_2$
985–1040	LT-$Ba_2Cu_3O_6$, ($\frac{1}{2}$)	CaO, (1)	$Ba_2CuO_{3.4}$ ($\frac{3}{2}$)	
1040				LT-$Ba_2Cu_3O_6 \Rightarrow$ HT-$Ba_2Cu_3O_{6-\delta} + x\ O_2$
1040–1055	HT-$Ba_2Cu_3O_6$, ($\frac{1}{2}$)	CaO, (1)	$Ba_2CuO_{3.4}$ ($\frac{3}{2}$)	
1055				$\frac{1}{2}Ba_2CuO_{3+\delta} + \frac{1}{2}HT - Ba_2Cu_3O_{6-\delta} \Rightarrow 2BaCuO_2 + xO_2$
1055–1065	CaO, (1)	$Ba_2CuO_{3.4}$, (1)	$BaCuO_2$ (2)	
1065				$Ba_2CuO_{3.4} + CaO + 2\ BaCuO_2 \Rightarrow$ cubic $Ba_4CaCu_3O_{8+\delta} + x\ O_2$
1065–1430	$Ba_4CaCu_3O_{8+\delta}$			
1430				Cubic $Ba_4CaCu_3O_{8+\delta} \Rightarrow$ Liquid $+ x\ O_2$

Between parentheses are the numbers of moles of each compound for 1 mole of $Ba_4CaCu_3O_{8+\delta}$ at the beginning of the experiment.

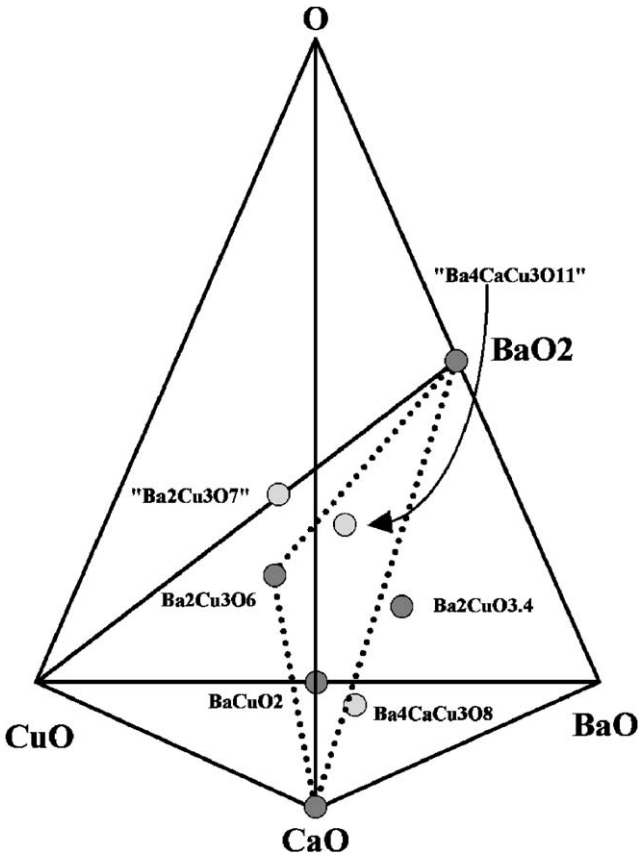

Fig. 8. Composition pyramid indicating the phases involved in the decomposition of $Ba_4CaCu_3O_{8+\delta}$ below 1065 K in $p(O_2) = 1$ bar and the plane delimited by the solid phases in equilibrium with the oxygen gas below 985 K (CaO, BaO_2, $Ba_2Cu_3O_6$; dotted lines). The overall composition is then "$Ba_4CaCu_3O_{11}$".

4. Discussion

4.1. Crystal structure of cubic and tetragonal $Ba_4CaCu_3O_{8+\delta}$

The crystal structure of cubic $Ba_4CaCu_3O_{8+\delta}$ as deduced from earlier reports [1,4,11] has been described in the introduction and the present refinement yielded the same results within standard uncertainties. It gives an oxygen composition of $z = 8.68$ and an average valence of +2.51 per copper atom. The Ca–O distance is equal to 2.277(3) Å. This is smaller than the sum of the relevant ionic radii, 1.00 Å for Ca^{2+} (VI) and 1.35 Å for O^{2-} (II) [22], indicating that the Ca–O bonds are compressed. As expected, the bond valence sum (BVS) for Ca [23], $\sum\exp\{(r_0-r)/B\} = \sum\exp\{(1.967-r)/0.37\} = 2.46$, is found significantly larger than 2. On the contrary, the Ba–O bonds are stretched with a mean Ba–O distance of 2.89 Å to be compared with the sum of the Ba^{2+} (IX) (1.47 Å) and the O^{2-} (II) ionic radii which is equal to 2.82 Å. In this case, the BVS [23], $\sum\exp\{(2.285-r)/0.37\} = 1.71$, is significantly lower than 2. This analysis may question the validity of the structure model but as no improvement could be made with other space groups, we believe that the discrepancies between the BVSs and the true oxidation states of Ba and Ca really represent strain in the structure. The main difference with $Ba_4RECu_3O_{8+\delta}$ (RE = Y, Ho, Er, Tm, Yb, Dy) [5,20,21] lies in the oxygen order. In the structure of the latter compounds (space group P-3m or P2-3), the half occupied O2 site is split into two sites, 6(f) $x0\frac{1}{2}$ with nearly full occupancy and 6(g) $x\frac{1}{2}0$ with only a residual

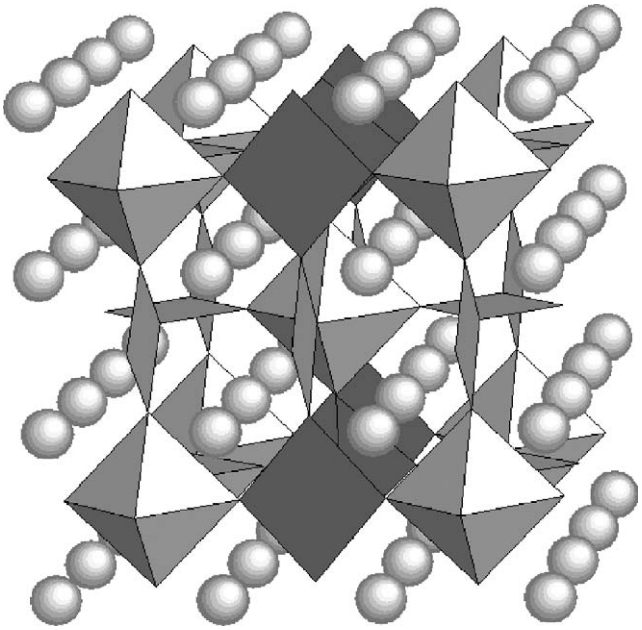

Fig. 9. Schematic representation of the structure of *RE*-413 (*RE* = Y, Ho, Er, Tm, Yb, Dy), space group *P*-3*m* or *P*2-3. CuO_4 squares: dark grey; CaO_6 octahedra and Ba atoms: light grey.

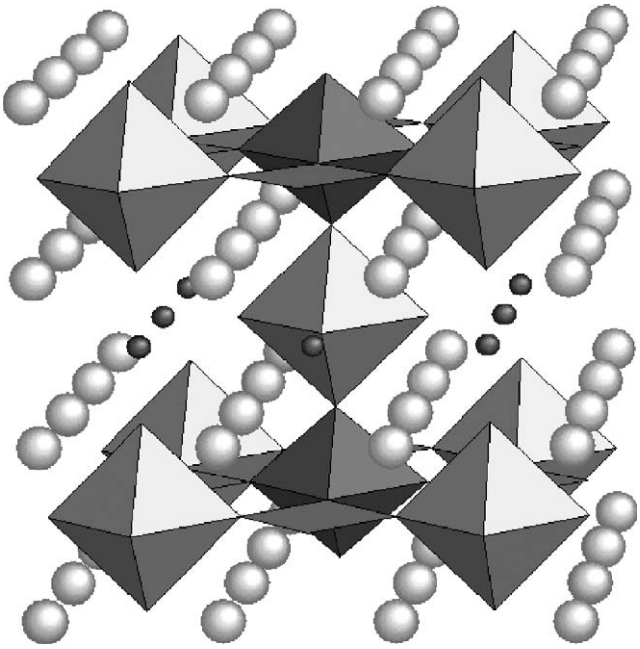

Fig. 10. Schematic representation of the structure of tetragonal $Ba_4CaCu_3O_{8+\delta}$. Cu atoms and CuO_z coordination polyhedra: dark grey; CaO_6 octahedra and Ba atoms: light grey.

occupancy. This results in a true four-fold square planar coordination (4*s*) for copper atoms as shown in Fig. 9. When the rare earth is Gd, Eu or Sm, both oxygen sites are half occupied [20,21]. In this case, the difference with the structure of cubic $Ba_4CaCu_3O_{8+\delta}$ is tenuous and is only caused by extremely small atom displacements. It is worth mentioning that strain is also present in the structure of *RE*-413. As an example, the BVSs for Ba and Y atoms in $Ba_4YCu_3O_{8.5}$ (space group *Pm*-3), calculated from data given in Ref. [5], are found equal to 1.76 and 3.95, respectively. For the composition $Ba_4YCu_3O_9$, the BVSs are 1.84 and 3.47, respectively, indicating a reduced strain when the oxygen content is increased.

A schematic drawing of the unit cell of tetragonal $Ba_4CaCu_3O_{8+\delta}$ is shown in Fig. 10. The main difference with the structure of cubic $Ba_4CaCu_3O_{8+\delta}$ lies in the reduced occupancy of some oxygen sites which is reflected in the overall oxygen content, 7.19, and in the cation coordination (Table 3). The 4(*m*) site (x, 0, $\frac{1}{2}$ with $x \approx 0.25$) is empty while the 4(*i*) site, split in 16(*u*), has only a residual occupancy which is neglected in the following discussion. The copper atoms in Cu1 and Cu4 sites have now a two-fold coordination with two collinear oxygen atoms (2*l*). The copper atoms in Cu2 site remain in a six-fold octahedral coordination (6*o*) with partially occupied neighbouring O sites (ACN = 4.44). Finally, the copper atoms in Cu3 site have now a four-fold square planar coordination (4*s*) with again a partial occupancy of the neighbouring O sites (ACN = 3.33). The Cu1–O and Cu4–O distances indicate that these two cations have an oxidation state close to +1: the sum of the relevant ionic radii, 0.46 Å for Cu^+ (II) and 1.35 for O^{2-} (II), is equal to 1.81 Å when the distances are found between 1.79 and 1.80 Å. In addition, the BVSs for Cu1 and Cu4, calculated with $r_0 = 1.610$ Å for Cu^+–O^{2-} [23], are 1.17 and 1.25, respectively. The mean Cu2–O distance, found equal to 2.03 Å, is close to the sum of $R(Cu^{2+}(VI)) = 0.73$ Å and $R(O^{2-}(II) = 1.35$ Å. Similarly, the mean Cu3-O distance, 1.88 Å, well compares to $R(Cu^{2+}(IV)) + R(O^{2-}(II) = 0.57 + 1.35 = 1.92$ Å. The copper atoms in sites Cu2 and Cu3 are therefore believed to be in an oxidation state close to +2 which is confirmed by BVS calculations with $r_0 = 1.679$ Å for Cu^{2+}–O^{2-} [23]: BVS(Cu2) = 1.90 and BVS(Cu3) = 1.96. These results are consistent with an average oxidation state for copper atoms of 1.49. The analysis of the Ba–O and Ca–O distances reveals the same tendency than in cubic $Ba_4CaCu_3O_{8+\delta}$ i.e. stretched Ba–O bonds and compressed Ca–O bonds with BVSs for Ba, Ca1 and Ca_2 of 1.48, 2.59 and 2.59, respectively.

4.2. Stability and formation of $Ba_4CaCu_3O_{8+\delta}$ in $p(O_2) = 1$ bar

In order to understand the behaviour of the BaO–CaO–CuO system and the stability of the $Ba_4CaCu_3O_{8+\delta}$ phase under a given oxygen partial pressure, the Gibbs phase rule is a useful tool. The degree of freedom (or variance) of a chemical system is given by

$$V = E + 2 - C$$

with E being the number of elements and C the constraints imposed to the system (temperature, pressure, phases which are present,…). In the case of BaO–CaO–CuO, E equals 4 which results in $6-C$ degrees of freedom. In the DTA/TG or neutron experiment, two parameters have been fixed: the temperature at a given time (heating rate) and the overall pressure which has been set to 1 bar of oxygen. The remaining variance is therefore 4, which means a maximum number of three condensed phases are in equilibrium with the gas phase. Using this argument, two different transformation reactions are possible in chemical systems with gaseous elements: those which are independent of the applied pressure (allotropic transformations, i.e. the phase has the same composition before and after the transformation or reaction among condensed species only) and those which include the gas phase in the reaction and therefore depend on the gaseous partial pressure of the involved gas species.

In the present case, the observed reactions are clearly of the second type. $Ba_4CaCu_3O_{8+\delta}$ is stable at $p(O_2) = 1$ bar between 1065 and 1430 K. It is not completely clear from our observations if the melting is congruent with respect to the metallic elements (which means only oxygen loss) or of the peritectic type with formation of CaO and/or BaO. The formed liquid reacts with the alumina crucible and has a strong creeping tendency which makes even qualitative statements on the type of reaction difficult. However, one can clearly state that the melting temperature is lowered by lowering the oxygen partial pressure. The decomposition at 1065 K is eutectoid with a measurable weight gain. $Ba_4CaCu_3O_{8+\delta}$ can therefore be stabilised by lowering the oxygen partial pressure; however, the oxygen content of the phase will vary. Indeed, $Ba_4CaCu_3O_{8+\delta}$ is stable down to room temperature in $p(O_2) < 10^{-6}$ bar with a tetragonal structure resulting from a significantly lower O content.

All other observed reactions include only Ba, Cu and O and are therefore identical to those observed in the ternary Ba–Cu–O system [24]. CaO is only acting as an inert additional component in that case. The maximum oxygen content in the multi-phase mixture is reached when BaO_2 appears for temperatures below 985 K. It is close to 11 oxygen atoms per formula unit (Fig. 8).

5. Conclusion

Neutron powder diffraction—high resolution and in situ experiments—and DTA/TGA have been used to study the crystal structure and stability of $Ba_4CaCu_3O_{8+\delta}$. We found that $Ba_4CaCu_3O_{8+\delta}$ has a tetragonal structure ($P4/mmm$, $a = 8.1976(3)$ Å, $c = 8.0709(3)$ Å) when it is prepared in reduced oxygen pressure ($p(O_2) < 10^{-6}$ bar). The difference with the cubic structure reported earlier lies in the reduced oxygen content which affects both the copper coordination and the copper formal valence. In the tetragonal structure, the copper atoms are either in a $+1$ or in a $+2$ oxidation state which results in average valence of $+1.5$ to be compared to $+2.5$ in the cubic structure. $Ba_4CaCu_3O_{8+\delta}$ is not stable below 1065 K in $p(O_2) = 1$ bar. In the case of a very dense ceramic, it remains in a metastable state down to room temperature. Otherwise, it undergoes a eutectoid decomposition into $Ba_2CuO_{3.4}$, CaO and $BaCuO_2$ with a measurable weight gain. It can therefore be stabilised by lowering the oxygen partial pressure, however, the oxygen content of the phase will vary. Indeed, $Ba_4CaCu_3O_{8+\delta}$ is stable down to room temperature in $p(O_2) < 10^{-6}$ bar with the tetragonal structure.

Below 985 K, the equilibrium in $p(O_2) = 1$ bar involves BaO_2, CaO and the low temperature form of $Ba_2Cu_3O_6$. The sequence of transformations between 985 and 1065 K have been established by in situ neutron powder diffraction.

The similarity between $Ba_4CaCu_3O_{8+\delta}$ and $Ba_4YCu_3O_{8+\delta}$ led us to investigate a possible transformation from a cubic to a tetragonal structure when the O content is lowered in the latter compound. Indeed, preliminary results indicate that $Ba_4YCu_3O_{8+\delta}$ has also a tetragonal structure when it is prepared at low oxygen pressure with $a = 8.199(2)$ Å and $c = 8.075(4)$ Å.

Acknowledgments

The authors gratefully acknowledge the financial support by the Région Rhône-Alpes through the "Avenir" program "TOSCA".

References

[1] C. Greaves, P.R. Slater, Solid State Commun. 73 (1990) 629–632.
[2] K.A. Kubat-Martin, E. Garcia, D.E. Peterson, Physica C 172 (1990) 75–80.
[3] F. Abbatista, A. Delmastro, D. Mazza, M. Valino, Mater. Chem. Phys. 28 (1991) 33–41.
[4] K.A. Kubat-Martin, G.H. Kwei, A.C. Lawson, D.E. Peterson, J. Solid State Chem. 100 (1992) 130–135.
[5] D.M. de Leeuw, C.A.H.A. Mutsaers, R.A. Steeman, E. Frikkee, H.W. Zandbergen, Physica C 158 (1989) 391–396.
[6] F. Abbatista, M. Vallino, D. Mazza, Mater. Chem. Phys. 21 (1989) 521–528.
[7] N.-L. Wu, E. Ruckenstein, Mater. Lett. 7 (1988) 169–171.
[8] S.-H. Lin, N.-L. Wu, Physica C 262 (1996) 33–44.
[9] H. Nguyen Xuan, Ch. Bertrand, S. Beauquis, A. Pisch, Ph. Galez, J. Phys. IV 122 (2004) 129–134.
[10] T.K. Jondo, S. Phok, Ph. Galez, J.L. Jorda, Crys. Eng. 5 (2002) 419–425.
[11] H. Nguyen Xuan, Ph. Galez, Ch. Bertrand, S. Beauquis, Mater. Lett. 59 (2005) 313–318.
[12] J. Rodriguez-Carvajal, Fullprof, 2000. Laboratoire Léon Brillouin, CEA-CNRS, Saclay, France.

[13] J.G. Thompson, T.J. White, R.L. Withers, J.D. Fitz Gerald, P.J. Barlow, S.J. Collocott, Mater. Forum 14 (1990) 27–32.
[14] E.L. Brosha, F.H. Garzon, I.D. Raistrick, P.K. Davies, J. Solid State Chem. 122 (1996) 176–185.
[15] F. Abbattista, M. Vallino, C. Brisi, M. Lucco-Borlera, Mater. Res. Bull. 23 (1988) 1509–1520.
[16] D. Richard, M. Ferrand, G.J. Kearley, Large Array Manipulation Program (LAMP), Available at Ftp://Ftp.ILL.fr/pub/cs.
[17] C. Greaves, P.R. Slater, Physica C 175 (1991) 172–178.
[18] M. Kikuchi, E. Ohshima, T. Atou, Y. Syono, Physica C 232 (1994) 263–268.
[19] M. Kikuchi, F. Izumi, E. Ohshima, Y. Morii, Y. Shimojo, Y. Syono, Physica C 247 (1995) 183–188.
[20] Y.T. Zhu, L. Shu, E.J. Peterson, D.E. Peterson, F.M. Mueller, J. Phys. Chem. Solids 63 (2002) 23–29.
[21] Y.T. Zhu, E.J. Peterson, P.S. Baldonado, J.Y. Coulter, D.E. Peterson, F.M. Mueller, J. Mater. Res. 14 (1999) 334–339.
[22] R.D. Shannon, Acta Cryst. A 32 (1976) 751–767.
[23] A.S. Wills, I.D. Brown, *VaList*, CEA, France, Program available from authors at willsas@netscape.net, 1999.
[24] S. Phok, Ph.D. Thesis, Université de Savoie, Annecy, France, 2002.